The Astrophysical Journal, 632:283–293, 2005 October 10

LATE-TIME X-RAY, UV, AND OPTICAL MONITORING OF SUPERNOVA 1979C

Stefan Immler,[1,2] Robert A. Fesen,[3] Schuyler D. Van Dyk,[4] Kurt W. Weiler,[5] Robert Petre,[1]
Walter H. G. Lewin,[6] David Pooley,[7] Wolfgang Pietsch,[8] Bernd Aschenbach,[8]
Molly C. Hammell,[3] and Gwen C. Rudie[3]

Received 2005 March 30; accepted 2005 June 19

ABSTRACT

We present results from observations of supernova (SN) 1979C with the *Newton X-Ray Multi-Mirror* (*XMM-Newton*) mission in X-rays and in UV, archival X-ray, and *Hubble Space Telescope* (*HST*) data, and follow-up ground-based optical imaging. The *XMM-Newton* MOS spectrum shows the best-fit two-temperature thermal plasma emission characteristics of both the forward ($kT_{\rm high} = 4.1^{+76}_{-2.4}$ keV) and reverse shock ($kT_{\rm low} = 0.79^{+0.24}_{-0.17}$ keV) with no intrinsic absorption. The long-term X-ray light curve, constructed from all X-ray data available, reveals that SN 1979C is still radiating at a flux level similar to that detected by *ROSAT* in 1995, showing no sign of a decline over the last 6 years, some 16–23 yr after its outburst. The high inferred X-ray luminosity ($L_{0.3-2} = 8\times10^{38}$ ergs s^{-1}) is caused by the interaction of the SN shock with dense circumstellar matter, likely deposited by a strong stellar wind from the progenitor with a high mass-loss rate of $\dot{M} \approx 1.5\times10^{-4}\ M_\odot$ yr^{-1} (v_w/10 km s^{-1}). The X-ray data support a strongly decelerated shock and show a mass-loss rate history that is consistent with a constant progenitor mass-loss rate and wind velocity over the past $\gtrsim$16,000 yr in the stellar evolution of the progenitor. We find a best-fit circumstellar medium (CSM) density profile of $\rho_{\rm CSM} \propto r^{-s}$ with index $s \lesssim 1.7$ and high CSM densities ($\gtrsim10^4$ cm^{-3}) out to large radii from the site of the explosion ($r \gtrsim 4\times10^{17}$ cm). Using *XMM-Newton* Optical Monitor data, we further detect a pointlike optical/UV source consistent with the position of SN 1979C, with *B*-, *U*-, and UVW1-band luminosities of 5, 7, and 9×10^{36} ergs s^{-1}, respectively. The young stellar cluster in the vicinity of the SN, as imaged by the *HST* and follow-up ground-based optical imaging, can only provide a fraction of the total observed flux, so that a significant contribution to the output likely arises from the strong interaction of SN 1979C with dense CSM.

Subject headings: circumstellar matter — galaxies: individual (M100, NGC 4321) — supernovae: individual (SN 1979C) — ultraviolet: ISM — X-rays: general — X-rays: individual (M100, NGC 4321, SN 1979C) — X-rays: ISM

Online material: color figure

1. INTRODUCTION

The interaction of the outgoing supernova (SN) shock and ejecta with the circumstellar medium (CSM) can produce substantial amounts of X-ray emission. The dominant X-ray production mechanism is the interaction of the SN shock with the ambient CSM deposited by either a pre-SN stellar wind or nonconservative mass transfer to a companion. This interaction produces hot gas with a characteristic temperature in the range $T \sim 10^7$–10^9 K (Chevalier & Fransson 1994). Gas heated to such a high temperature produces radiation predominantly in the X-ray range. X-ray emission from this interaction is expected for all Type Ib/c and II SNe with substantial CSM established by the massive progenitors. The details of the CSM interaction are discussed in Fransson et al. (1996 and references therein), while the X-ray interaction luminosity is briefly summarized here (see also Immler & Lewin 2003).

The thermal X-ray luminosity, $L_{\rm X}$, produced by the shock-heated CSM, can be expressed as $L_{\rm X} = 4/(\pi m^2)\Lambda(T)(\dot{M}/v_w)^2 (v_s t)^{-1}$, where m is the mean mass per particle (2.1×10^{-27} kg for a H+He plasma), $\Lambda(T)$ is the cooling function of the heated plasma at temperature T, $\dot{M}$ is the mass-loss rate of the progenitor, v_w is the speed of the stellar wind blown off by the progenitor, and v_s is the speed of the outgoing shock. If X-ray spectroscopic data are available, $\Lambda(T)$ is known, and the interaction luminosity $L_{\rm X}$ at time t after the outburst can be used to measure the ratio $\dot{M}/v_w$. Assuming a constant SN shock velocity v_s, the shock will reach a radius of $r = v_s t$ from the site of the explosion at time t after the explosion.

If the CSM density $\rho_{\rm CSM}$ is dominated by a wind from the progenitor of the SN, the continuity equation requires $\dot{M} = 4\pi r^2 \rho_w(r) v_w(r)$ through a sphere of radius r, where ρ_w is the stellar wind density. After the SN shock plows through the CSM, its density is $\rho_{\rm CSM} = 4\rho_w$ (Fransson et al. 1996), assuming no losses to cosmic-ray acceleration.

Since each X-ray measurement at time t is related to the corresponding distance r from the site of the explosion, which has been reached by the wind at a time depending on v_w, or the age of the wind $t_w = t v_s/v_w$, we can use our measurements as a "time machine" to probe the progenitor's history over significant timescales. Assuming that v_w and v_s did not change over t_w, or in cases where the shock front deceleration is known from radio data, we can even directly measure the mass-loss rate back

[1] Exploration of the Universe Division, X-Ray Astrophysics Laboratory, Code 662, NASA Goddard Space Flight Center, Greenbelt, MD 20771; immler@milkyway.gsfc.nasa.gov.
[2] Universities Space Research Association.
[3] Department of Physics and Astronomy, 6127 Wilder Laboratory, Dartmouth College, Hanover, NH 03755.
[4] *Spitzer* Science Center, Caltech, MS 220-6, Pasadena, CA 91125.
[5] Naval Research Laboratory, Code 7213, Washington, DC 20375-5320.
[6] Center for Space Research, Massachusetts Institute of Technology, 77 Massachusetts Avenue, Cambridge, MA 02139.
[7] Department of Astronomy, University of California, 601 Campbell Hall, Berkeley, CA 94720-3411.
[8] Max-Planck-Institut für extraterrestrische Physik, Postfach 1312, 85741 Garching bei München, Germany.

in time. Furthermore, integration of the mass-loss rate along the path of the expanding shell gives the mean density inside a sphere of radius r. For a constant wind velocity v_w and constant mass-loss rate $\dot{M}$, a $\rho_{\rm CSM} = \rho_0(r/r_0)^{-s}$ profile with $s = 2$ is expected.

After the expanding shell has become optically thin, it is expected that emission from the SN ejecta itself, heated by the reverse shock, dominates the X-ray output of the interaction regions due to its higher emission measure and higher density. Since the plasma temperature of the ejecta is lower than that of the shocked CSM, a significant "softening" of the X-ray spectrum is expected (e.g., Chevalier & Fransson 1994; Fransson et al. 1996).

The number of detected X-ray SNe has grown substantially over the past few years. With 23 detections to date[9] and high-quality X-ray spectra available from the *Newton X-Ray Multi-Mirror* (*XMM-Newton*) mission and *Chandra X-Ray Observatory* observations, a wealth of new information has been gathered (see Immler & Lewin [2003] for a review).

The signatures of circumstellar interaction in the radio, optical, and X-ray regimes have been found for a number of core-collapse SNe, such as the Type II-L SN 1979C (e.g., Weiler et al. 1986, 1991; Fesen & Matonick 1993; Immler et al. 1998). SN 1979C was discovered in the optical near maximum light on 1979 April 19 (Mattei et al. 1979) and detected in X-rays 16 yr after its outburst with the *Röntgensatellit* High Resolution Imager (*ROSAT* HRI), with a luminosity of $L_{0.1-2.4} = 1.3 \times 10^{39}$ ergs s^{-1} (Immler et al. 1998). The *ROSAT* data imply a mass-loss rate of $\dot{M} \sim 1 \times 10^{-4}\ M_\odot\ {\rm yr}^{-1}\ (v_w/10\ {\rm km\ s}^{-1})$, similar to the mass-loss rates of other massive ($\gtrsim 10\ M_\odot$) SN progenitors (e.g., SNe 1978K, 1986J, 1988Z, and 1998S) and in agreement with the mass-loss rate inferred from Very Large Array[10] radio observations [$\dot{M} = 1.2 \times 10^{-4}\ M_\odot\ {\rm yr}^{-1}\ (v_w/10\ {\rm km\ s}^{-1})$; Weiler et al. 1991]. Earlier *Einstein* observations only gave an upper limit to the X-ray luminosity on days 64, 239, and 454 after the outburst, with 3 σ upper limits of 1.8×10^{40}, 7.6×10^{39}, and 6.9×10^{39} ergs s^{-1}, respectively (Immler et al. 1998). Since the *ROSAT* HRI instrument does not provide energy information, and subsequent *Advanced Satellite for Cosmology and Astrophysics* (*ASCA*) and *Chandra* observations (Kaaret 2001; Ray et al. 2001) lacked enough photon statistics for X-ray spectroscopy, there is no information about the X-ray spectral properties of SN 1979C and hence the temperatures of the forward and reverse shock.

SN 1979C was extensively monitored in the radio starting 8 days after maximum light and showed an initial rate of decline of $t^{-0.7}$ (Weiler et al. 1986, 2001), followed by a flattening or possibly brightening at an age of $\approx$10 yr, while maintaining a relatively constant spectral index (Montes et al. 2000; Weiler et al. 2001). The results were interpreted as being due to a denser region in the CSM or a complex CSM structure that might have been modulated by the stellar wind of the progenitor's companion (Weiler et al. 1992).

There are conflicting reports in the literature regarding the expansion velocity of the ejecta. While Bartel & Bietenholz (2003) find a near-free expansion [i. e., $E(T, V) = $ const.] based on Very Long Baseline Array (VLBI) data from $t = 3.7-22$ yr after the explosion, Marcaide et al. (2002) report the detection of a strongly decelerated expansion. There is consensus, however, that the initial expansion of the shock over the first 6 ± 2 yr was free, with $v_s \approx 9000$ km s^{-1} (see Marcaide et al. 2002 and references therein). The claimed onset of the deceleration to $v_s \approx 6200$ km s^{-1} coincides with the flattening of the radio light curve and might be indicative of the shock running into a dense CSM (Marcaide et al. 2002).

Low-dispersion Keck optical spectra obtained at $t = 14.8$ and 17 yr, as well as *Hubble Space Telescope* (*HST*) UV spectra 17 yr after the outburst, revealed broad $\approx$6000 km s^{-1} emission lines, with stronger blueward emission peaks than redward ones suggesting internal dust extinction within the expanding ejecta. Profile differences between hydrogen and oxygen line emission suggest two or more separate emitting regions, such as a Hα bright shell and oxygen inner ejecta region (Fesen et al. 1999).

HST imaging of the SN 1979C environment showed the presence of a cluster of stars in the vicinity of SN 1979C, containing both young ($\approx$4–8 Myr) blue stars and older red supergiants ($\approx$20 Myr), and succeeded in identifying SN 1979C as the brightest source in the optical and UV in that cluster (van Dyk et al. 1999). The data were further used to estimate the mass of the progenitor to be $18 \pm 3\ M_\odot$, in agreement with a mass estimate derived from radio data ($\gtrsim 13\ M_\odot$; Weiler et al. 1991).

In this paper we report on *XMM-Newton* X-ray and UV observations of SN 1979C, all archival X-ray data available, as well as archival *HST* images and new ground-based optical data. In § 2 we describe the data and analysis thereof and report on the X-ray spectrum, multimission X-ray light curve, UV photometry, and new follow-up ground-based optical imaging in § 3. We discuss the results in the context of the CSM interaction model and compare them to other core-collapse SNe in § 4, followed by a brief summary in § 5.

2. DATA PROCESSING AND ANALYSIS

SN 1979C and its host galaxy NGC 4321 (M100) were observed with *XMM-Newton* as part of a GTO program on 2001 December 28, with the European Photon Imaging Camera (EPIC) pn instrument for 31.6 ks and the EPIC MOS1 and MOS2 instruments for 36.2 and 36.0 ks, respectively, using the medium filter. Data processing and analysis were performed with SAS, version 6.1, and the latest calibration constituents, as well as FTOOLS and our own IDL routines. Spectral fitting was performed using XSPEC, version 12.2.0.

In order to establish the long-term X-ray light curve of SN 1979C, we further extracted and reduced all X-ray data available in the archives (see § 2.3). *XMM-Newton* Optical Monitor (OM) data of SN 1979C (§ 2.2), as well as archival *HST* and recent MDM observations (§ 2.4), were further used to estimate optical/UV fluxes.

2.1. *XMM-Newton EPIC Data*

Screening of the pn and MOS data for periods with a high background revealed contamination of the data at the end of the observation period. Exclusion of these flaring periods gave cleaned exposure times of 27.1 ks (pn) and 23.6 ks (MOS).

Inspection of the EPIC images further showed that the position of SN 1979C coincides with a chip gap on the pn detector, making a reliable count rate estimate impossible. The pn data were therefore not used in the analysis, and we restrict ourselves to the EPIC MOS data only. The MOS data were further screened using the parameters "FLAG = 0" and "PATTERN <= 12" and filtered to retain the 0.3–10 keV energy band only in order

[9] A complete list of X-ray SNe and references are available at http://lheawww.gsfc.nasa.gov/users/immler/supernovae_list.html.

[10] The VLA is operated by the National Radio Astronomy Observatory, which is a facility of the National Science Foundation, operated under cooperative agreement by Associated Universities, Inc.

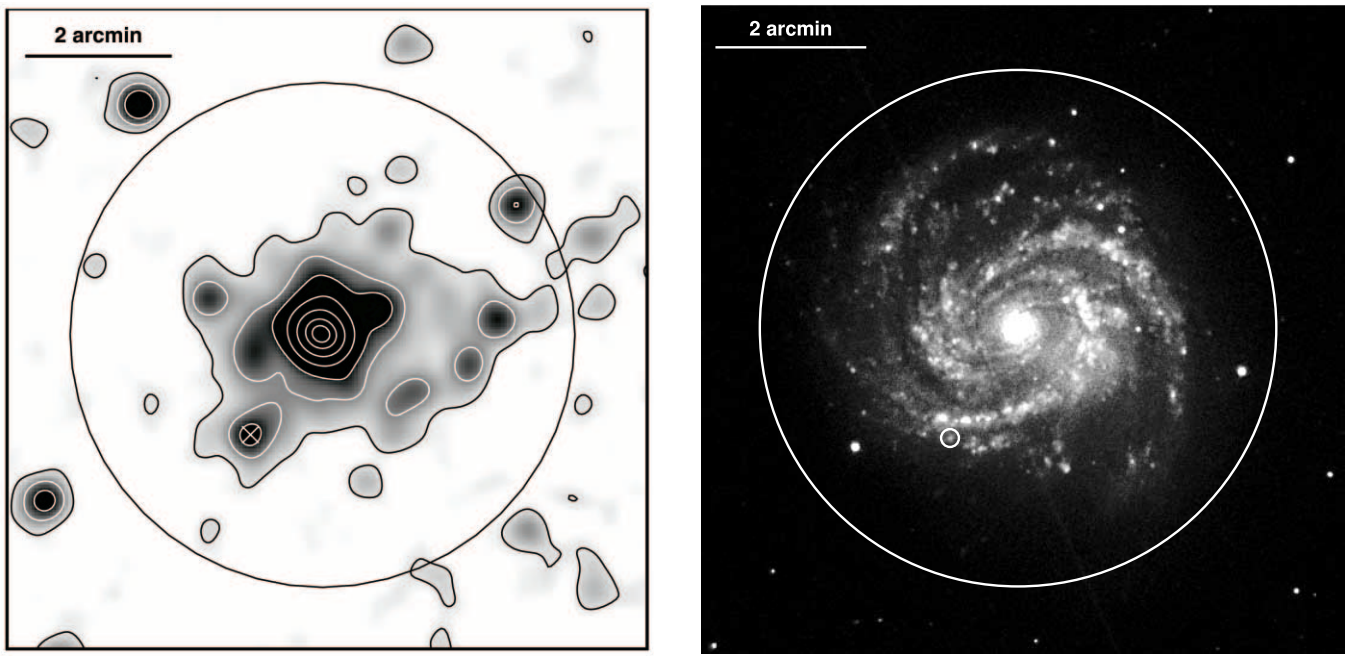

FIG. 1.—*Left*: Merged *XMM-Newton* EPIC MOS1+MOS2 image of M100 and SN 1979C in the 0.3–10 keV band in logarithmic gray scale. The image was adaptively smoothed to achieve a signal-to-noise ratio of 10. Contour lines are 0.65 (*black*), 1, 1.5, 3, 6, 10, and 13×10^{-5} counts s^{-1} $pixel^{-1}$. The position of SN 1979C is marked by a white cross. The black circle gives the D_{25} ellipse of M100. *Right*: *B*, *U*, and UVW1 OM image of M100. The small white circle (radius 7″.5) is centered on the radio position of SN 1979C. The large white circle indicates the D_{25} ellipse of M100 as in the left panel. [*See the electronic edition of the Journal for a color version of Fig. 1b*.]

to avoid contamination from soft proton flaring and uncertainties in the calibration at low energies. The merged 0.3–10 keV band MOS1+MOS2 image of M100/SN 1979C is shown in the left panel of Figure 1. MOS counts were extracted within a circle of radius 30″ centered on the radio position of SN 1979C and corrected for the energy-enclosed aperture. The background was estimated locally from a source-free annulus with inner and outer radii of 45″ and 55″, respectively, to account for residual diffuse emission from the host galaxy.

2.2. *XMM-Newton Optical Monitor Data*

Optical Monitor data were obtained in 16 individual exposures in the *B* band (effective wavelength 4340 Å), *U* band (3440 Å), and UVW1 band (2910 Å), with on-source exposure times of 2.0 ks (*B*), 1.8 ks (*U*), and 1.9 ks (UVW1). OM data were reprocessed using the SAS `omichain` task and following the data analysis threads in the ABC Guide, version 2.01.[11]

For imaging and source detection, the tracking history was created, bad pixels were removed, a flat field generated, and images were corrected for "mod 8" spatial fixed pattern noise. Source detection was performed using the `omdetect` task, which employs a two-stage process to locate sources in OM Science Window images, i.e., determination of the background and consecutive island search (`boxdetect`) in which sets of pixels above the sigma significance cutoff are identified and grouped into individual objects. Source counts were converted into instrument-bandpass magnitudes using the `ommag` command. Fluxes were converted from count rates using a step-by-step recipe provided by Alice Breeveld.[12] We also employed the interactive `omsource` task with various aperture sizes to verify the magnitudes obtained with `omichain` and to check for potential contamination of the OM photometry with nearby sources.

Comparison of the optical positions of six stars from the Guide Star Catalog with the centroid positions of the stars in the *B*, *U*, and UVW1 images revealed an offset of individual OM images of ΔR.A. = 0″.14, Δdecl. = −0″.95 (*B*); ΔR.A. = 0″.43, Δdecl. = −1″.75 (*U*); and ΔR.A. = 1″.01, Δdecl. = −2″.23 (UVW1). This offset was also visible in an overlay of the *B*, *U*, and UVW1 images. After realignment of the images with shifts in right ascension and declination as quoted above, neither systematic offset between the different images nor statistically significant offset between the centroid positions of the stars with the Guide Star Catalog positions are observed.

A three-color (*B*, *U*, and UVW1) image of M100 and SN 1979C is shown in the right panel of Figure 1. The circular enhancement in the southwestern spiral arm of M100, most prominent in the *B*-band image (red in online edition), is due to stray light from the bright nucleus of M100. Due to its large offset from the position of SN 1979C and local background extraction, however, it does not affect the SN 1979C photometry. An *XMM-Newton* OM *U*-band image of the region around the position of SN 1979C is further shown in more detail in Figure 2 (*top panel*).

2.3. *Other X-Ray Data*

In addition to the *XMM-Newton* data described above, we used archival data from *Einstein* (HRI), *ROSAT* (HRI and PSPC), *ASCA* (Solid-State Imaging Spectrometer [SIS]), and a recent *Chandra* (ACIS-S) observation. All *Einstein* observations were merged into a single 41.2 ks observation to increase the photon statistics. Count rates from the archival *Einstein* HRI and *ROSAT* HRI observations were taken from Immler et al. (1998), *Chandra* count rates were taken from Ray et al. (2001) and Kaaret (2001), and *ASCA* upper limits were taken from Ray et al. (2001). We further extracted source counts for each of

[11] See http://heasarc.gsfc.nasa.gov/docs/xmm/abc.
[12] See http://xmm.vilspa.esa.es/sas/documentation/watchout/uvflux.shtml.

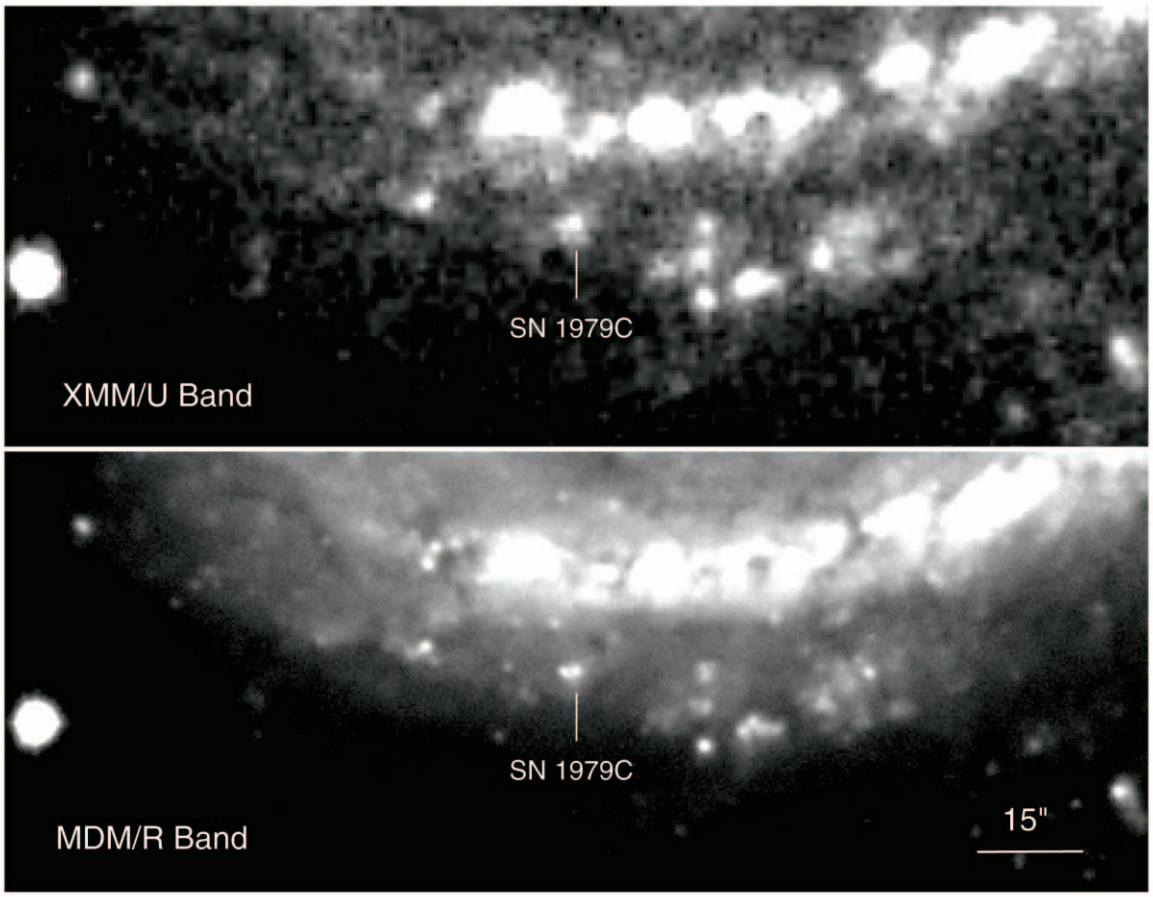

FIG. 2.—*XMM-Newton* OM *U*-band image (*top panel*) and MDM 2.4 m Hiltner Telescope *R*-band image of the southern spiral arm of M100 centered on the position of SN 1979C. The 15″ scale bar in the bottom panel applies to both panels.

these observations following standard analysis methods as described in the respective instrument handbooks using FTOOLS to check and reproduce published count rates. Two previously unpublished *ROSAT* HRI observations were analyzed, as described in Immler et al. (1998).

A *ROSAT* PSPC observation from 1998 December 8 was also used to establish the long-term X-ray light curve of SN 1979C. This observation was selected as part of the *ROSAT* PSPC "last-light" campaign during which the PSPC instrument was reactivated for a final set of observations just days before *ROSAT* was decommissioned. Inspection of the PSPC data showed that the position of SN 1979C was sufficiently offset from the "gain hole," which emerged on the PSPC-B detector images taken during the short last-light campaign. Exposure-corrected counts were extracted from the position of SN 1979C within a circle of radius 30″ and corrected for the 100% encircled energy radius. The background was estimated locally within an annulus of inner and outer radii of 1′ and 1.′3. The net exposure time of the observation is 7.8 ks. A log of all X-ray observations used in this paper is given in Table 1.

TABLE 1
X-RAY OBSERVATIONS OF SN 1979C

Mission	Instrument	Observation ID/Sequence Number	Date	Exposure (ks)	MJD
Einstein	HRI	H1220N16.XIA	1979 Jun 7	4.0	44,031
Einstein	HRI	H1220N16.XIB	1979 Dec 12	13.4	44,217
Einstein	HRI	H1220N16.XIC	1980 Jun 29	23.8	44,418
ROSAT	HRI	RH600731N00	1995 Jun 17	42.8	49,885
ROSAT	HRI	RH500422N00	1995 Jul 1	9.0	49,899
ASCA	SIS	55044000	1997 Dec 24	27.3	50,806
ROSAT	HRI	RH500542N00	1997 Dec 27	25.1	50,809
ROSAT	PSPC	RP180296N00	1998 Dec 8	7.8	51,155
Chandra	ACIS-S	700072	1999 Jun 11	2.5	51,340
XMM-Newton	MOS	0106860201	2001 Dec 28	36.6	52,271

NOTE.—All *Einstein* HRI observations were merged into a single 41.2 ks observation.

TABLE 2
OPTICAL/UV OBSERVATIONS OF SN 1979C

Telescope	Filter	Date	Exposure (ks)	MJD
HST WFPC2-PC1	*U* (F336W)	1996 Jul 29	2.6	50,293
	B (F439W)	1996 Jul 29	2.4	50,293
	R (F675W)	1996 Jul 29	1.0	50,293
	Hα (F658W)	1996 Jul 29	3.9	50,293
XMM-Newton OM	*U*	2001 Dec 28	1.8	52,271
	B	2001 Dec 28	2.0	52,271
	UVW1	2001 Dec 28	1.9	52,271
MDM Hiltner 2.4 m	*R*	2004 Dec 19	2.0	53,358
	Hα	2004 Dec 19	3.0	53,358

2.4. *Follow-up Ground-based Optical Imaging*

Hα and Harris *R*-band images were obtained at the MDM Observatory on 2004 December 19 and 20 (epoch = 2004.97 $\simeq$ 2005.0), using the Hiltner 2.4 m telescope and the Columbia 8 K CCD camera (Crotts 2001). The images were used to investigate further the nature of the source detected at the SN 1979C site and to compare more directly its current optical flux level with that seen in previous late-time optical detections (Fesen et al. 1999; van Dyk et al. 1999). Two 1000 s *R*-band and three 1000 s Hα exposures binned 2×2 yielding an image scale of 0.″404 pixel^{-1} were taken under poor to fair conditions. The Hα image had poor image quality (3″ FWHM), while the *R*-band images were fair to good (1.″2–1.″4 FWHM). These data were reduced, co-added, and cosmic-ray corrected using standard IRAF software routines. The MDM *R*-band image of the region around the position of SN 1979C is shown in Figure 2 (*bottom panel*).

As a means for comparison of current optical flux levels, we also retrieved and reprocessed the archival *HST* Wide Field Planetary Camera 1 (WFPC1) images of the SN 1979C region (cf. van Dyk et al. 1999). These data consist of several filter images taken 1996 July 29, using the WFPC2 camera with the SN 1979C site centered in the high-resolution Planetary Camera (PC1; 0.″046 pixel^{-1}). Two 500 s broadband red (F675W), three 1300 s Hα (F658N), two 1200 s *B*-band (F439W), and two 1300 s *U*-band (F336W) filter images were co-added and cosmic rays removed via a high pixel value rejection procedure. A few obvious residual cosmic-ray–contaminated pixels on the summed F675W image were also removed manually using the IRAF software package `tv.imedit`. All optical/UV observations used in this paper are listed in Table 2.

3. RESULTS

3.1. *X-Ray Data*

SN 1979C is detected in the MOS images with a count rate of $(3.6 \pm 0.5)\times10^{-3}$ counts s^{-1}, 23 yr after its outburst. Simultaneous spectral fitting of the MOS data in the 0.5–8 keV band gives a best-fit (reduced $\chi^2_r = 0.65$ for 18 degrees of freedom [dof]) two-temperature plasma emission model (XSPEC model MEKAL) with $kT_{\rm low} = 0.77^{+0.17}_{-0.19}$ and $kT_{\rm high} = 2.31^{+1.95}_{-0.66}$ keV, and a best-fit absorbing column density of $N_{\rm H} = 2.53^{+4.96}_{-2.53} \times 10^{20}$ cm^{-2} consistent with the Galactic foreground column density ($N_{\rm H} = 2.39 \times 10^{20}$ cm^{-2}; Dickey & Lockman 1990). Element abundances cannot be constrained due to the low photon statistics.

In order to avoid contamination of the spectra with unresolved and hard X-ray binaries (XRBs) within the disk of M100, we further fitted the spectrum in the 0.5–2 keV band, where the bulk of emission from the reverse shock is expected. A best-fit two-temperature thermal plasma emission model ($\chi^2_r = 0.61$, dof = 8) gives $kT_{\rm low} = 0.78^{+0.25}_{-0.17}$ and $kT_{\rm high} = 4.1^{+76}_{-2.3}$ keV, and an absorbing column density of $N_{\rm H} = (0\text{–}1.01)\times10^{21}$ cm^{-2}. The best-fit plasma temperatures are essentially unchanged if we set the absorbing column density to the Galactic foreground column density ($kT_{\rm low} = 0.79^{+0.24}_{-0.17}$ and $kT_{\rm high} = 4.1^{+76}_{-2.4}$ keV; $\chi^2_r = 0.60$, dof = 9). Adopting this spectral template gives 0.3–2 and 2–8 keV fluxes of $f_{0.3-2} = 2.28\times10^{-14}$ and $f_{2-8} = 1.97\times10^{-14}$ ergs cm^{-2} s^{-1}, respectively. The soft component contributes 64% to the total 0.3–2 keV band emission, while the hard component accounts for the remaining 36% of the soft-band flux. The MOS spectra and best-fit model are shown in Figure 3.

A single-component thermal plasma spectrum gives best-fit $kT = 0.60^{+0.12}_{-0.19}$ keV and an absorbing column density of $N_{\rm H} = 6.5^{+2.0}_{-1.9}\times10^{21}$ cm^{-2} ($\chi^2_r = 1.29$, dof = 11). If the absorbing column density is set to the Galactic foreground column density, a slightly higher plasma temperature is inferred ($kT = 0.85^{+0.25}_{-0.10}$ keV; $\chi^2_r = 1.73$). Using these spectral properties gives a soft-band flux of $f_{0.3-2} = 1.76\times10^{-14}$ ergs cm^{-2} s^{-1}. It should be noted, however, that such a model gives larger systematic residuals below $\approx$0.7 keV and above $\approx$1.5 keV.

A thermal bremsstrahlung spectrum with $kT = 0.53^{+1.40}_{-0.33}$ keV ($\chi^2_r = 0.91$, dof = 11) cannot be statistically ruled out but shows significantly larger systematical offsets from the observed spectrum, especially at lower energies. Adopting this spectral template gives a soft-band flux of $f_{0.3-2} = 2.11\times10^{-14}$ ergs cm^{-2} s^{-1}.

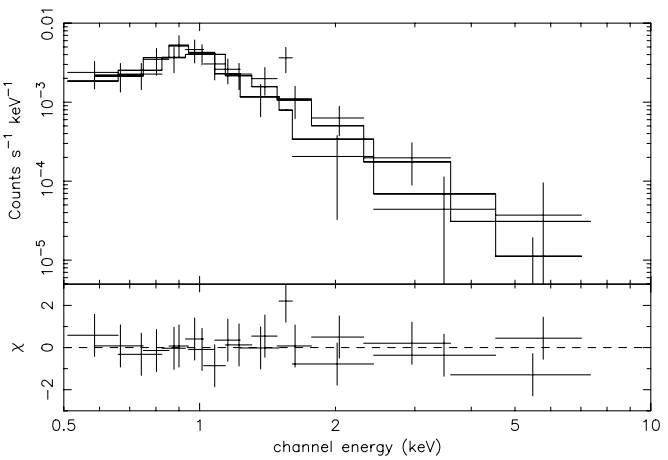

FIG. 3.—EPIC MOS1 and MOS2 X-ray spectra of SN 1979C (*top panel*). The bottom panel shows the residuals of the fits in units of σ for the best-fit spectral model consisting of a two-component thermal plasma emission model (see § 3.1).

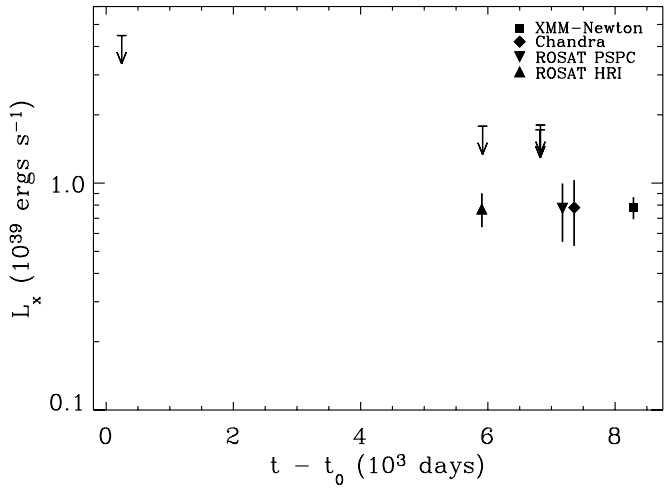

FIG. 4.—Soft (0.3–2 keV) band X-ray light curve of SN 1979C based on *Einstein*, *ROSAT*, *ASCA*, *Chandra*, and *XMM-Newton* data. Upper limits are from *Einstein* HRI, *ROSAT* HRI, and *ASCA* SIS observations. Time is given in units of 10^3 days after the outburst of SN 1979C (see Table 1).

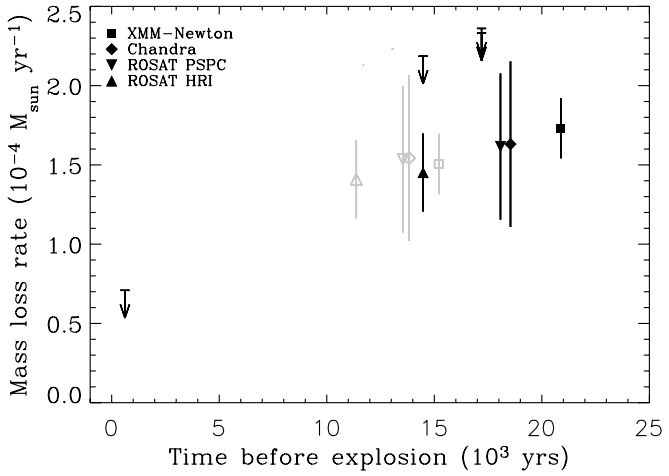

FIG. 5.—Mass-loss rate history of SN 1979C as a function of the stellar wind age, in units of 10^3 yr before the explosion, for a constant shock velocity (*filled black symbols*) and for a decelerated shock (*open gray symbols*; see Table 1 and § 3.1).

Other spectral models, such as a power law ($\Gamma = 4.48^{+0.53}_{-0.48}$; $\chi^2_r = 0.87$, dof = 17) or a nonequilibrium ionization model ($kT = 73.4^{+6.5}_{-33.0}$ keV; $\chi^2_r = 0.93$, dof = 16) cannot be statistically ruled but give unreasonable physical parameters.

Using the above two-temperature thermal plasma spectral template and assuming a distance of 17.1 Mpc (Freedman et al. 1994), we infer soft- and hard-band X-ray luminosities of $L_{0.3-2} = 8 \times 10^{38}$ and $L_{2-10} = 3 \times 10^{38}$ ergs s^{-1}, respectively.

We also analyzed the multimission data set to construct the long-term X-ray light curve of SN 1979C, using the same spectral template to convert count rates into fluxes and luminosities. The long-term X-ray light curve is shown in Figure 4. We calculated the mass-loss rate of the progenitor as a function of age of the stellar wind assuming a constant shock velocity of 9200 km s^{-1} (Marcaide et al. 2002). An effective (0.3–2 keV band) cooling function of $\Lambda = 3 \times 10^{-23}$ ergs cm^3 s^{-1} for an optically thin thermal plasma with a temperature of 10^7 K was adopted, which corresponds to the temperature inferred from the MOS spectra. Adopting different plasma temperatures in the range 0.5–1 keV would lead to changes in the emission measure of ≈10%. This error in the emission measure is included in calculations of the CSM number densities (§ 4.1). Key physical properties of SN 1979C are listed in Table 3.

While the mass-loss rate history (see Table 3 and Fig. 5) indicates a slight increase in the mass-loss rate toward a larger stellar wind age, the results are not statistically significant. We further calculated the mass-loss rate history assuming a strongly decelerated expansion of the shock of 9200 km s^{-1} for a stellar wind age of $t_w < 6$ yr, 6200 km s^{-1} for 6 yr $< t_w <$ 14 yr, and 5400 km s^{-1} for $t_w > 20$ yr, corresponding to a deceleration $R \propto t^m$ with a deceleration parameter of $m = 0.6$ (Marcaide et al. 2002) to approximate a continually decelerating shock (shown in gray scale in Fig. 5). The introduction of a deceleration leads to a constant mass-loss rate of $\dot{M} \approx 1.5 \times 10^{-4}\ M_\odot$ yr^{-1} (v_w/10 km s^{-1}).

We computed the CSM number density in the vicinity of the SN by integrating the mass-loss rate within the sphere probed by the CSM interaction. The postshock CSM number densities, $n = \rho_{\rm CSM}/m$, for the different radii $r = v_s t$ corresponding to the dates of the observations are listed in Table 3. An overall decrease in the CSM density is observed from $n = (1.17 \pm 0.32) \times 10^4$ cm^{-3} at $\log r$(cm) = 17.50 (*ROSAT* HRI) to $n = (0.85 \pm 0.19) \times 10^4$ cm^{-3} at $\log r$(cm) = 17.59 (*XMM-Newton*), albeit not statistically significant. While the *ROSAT* PSPC and *Chandra* data at $\log r$(cm) = 17.52 [$n = (1.66 \pm 0.63) \times 10^4$ cm^{-3}] and 17.53 cm [$n = (1.51 \pm 0.56) \times 10^4$ cm^{-3}]

TABLE 3
X-RAY PROPERTIES OF SN 1979C

Epoch (yr) (1)	Instrument (2)	$f_{0.3-2}$ (10^{-14} ergs cm^{-2} s^{-1}) (3)	$L_{0.3-2}$ (10^{39} ergs s^{-1}) (4)	$\dot{M}$ ($10^{-4}\ M_\odot$ yr^{-1}) (5)	$\log r$ (cm) (6)	t_w (yr) (7)	n (10^4 cm^{-3}) (8)
0.66.....	*Einstein* HRI	<12.78	<4.47	<0.71	16.28	615	<223.87
16.18.....	*ROSAT* HRI	2.20 ± 0.37	0.77 ± 0.13	1.45 ± 0.25	17.50	14,878	1.17 ± 0.32
16.22.....	*ROSAT* HRI	<5.09	<1.78	<2.19	17.51	14,914	<1.17
18.71.....	*ASCA* SIS	<4.92	<1.72	<2.33	17.51	17,200	<1.66
18.72.....	*ROSAT* HRI	<5.15	<1.80	<2.36	17.51	17,208	<1.66
19.67.....	*ROSAT* PSPC	2.21 ± 0.63	0.77 ± 0.22	1.62 ± 0.46	17.52	18,080	1.66 ± 0.63
20.17.....	*Chandra* ACIS-S	2.23 ± 0.71	0.78 ± 0.25	1.63 ± 0.52	17.53	18,546	1.51 ± 0.56
22.72.....	*XMM-Newton* MOS	2.28 ± 0.26	0.80 ± 0.09	1.75 ± 0.19	17.59	20,893	0.85 ± 0.19

NOTES.—Col. (1): Epoch after the peak optical brightness (1979 April 15) in units of yr. Col. (3): 0.3–2 keV X-ray band flux in units of ergs cm^{-2} s^{-1}. Col. (4): 0.3–2 keV X-ray band luminosity in units of ergs per second. Col. (5): Mass-loss rate of the progenitor in units of $M_\odot$ yr^{-1}. Col. (6): Log of the radius from the site of the explosion. Col. (7): Age of the stellar wind in units of years. Col. (8): Postshock CSM number density in units of 10^4 cm^{-3}.

are slightly higher, they are consistent with the earlier *ROSAT* HRI and later *XMM-Newton* data within the errors. The CSM density profile is discussed in more detail in § 4.1.

3.2. *XMM-Newton Optical Monitor Data*

An optical/UV source is found at the position of SN 1979C in the *B*, *U*, and UVW1 bands, with magnitudes of $m_B = 19.1 \pm 0.1$, $m_U = 18.0 \pm 0.1$, and $m_{\rm UVW1} = 17.6 \pm 0.1$ mag, and source detection significances of 17.1, 28.1, and 34.5 σ, respectively, within an aperture of 12 pixels (4.″1 FWHM). The source is flagged as pointlike by the source detection algorithm. Magnitudes were converted into fluxes with Vega as a reference (Vega has magnitudes of $m_B = 0.030$ and $m_U = m_{\rm UVW1} = 0.035$ mag) and a relation of $m_{\rm Vega} - m_{\rm SN1979C} = -2.5 \log (f_{\rm Vega}/f_{\rm SN1979C})$ and Vega fluxes in the OM *B*, *U*, and UVW1 filters of 5.97, 3.15, and 3.73×10^{-9} ergs cm^{-2} s^{-1} Å^{-1}. We obtain *B*-, *U*-, and UVW1-band fluxes for SN 1979C of 1.4, 2.0, and 3.3×10^{-16} ergs cm^{-2} s^{-1} Å^{-1}, respectively.

In order to minimize contamination of the optical/UV with potential unresolved neighboring sources, we also extracted OM counts within smaller apertures of 3 pixel radius (2.″9) from the centroid position of SN 1979C. Using this small aperture we obtain $m_{\rm UVW1} = (17.9 \pm 0.1)$ mag, $f_{\rm UVW1} = 2.6 \times 10^{-16}$ ergs cm^{-2} s^{-1} Å^{-1}, and $L_{\rm UVW1} = 9.0 \times 10^{36}$ ergs s^{-1}.

3.3. *R-Band and* Hα *Imaging*

Our 2005.0 MDM *R*-band image of the SN 1979C region in M100 is shown in Figures 2 and 7, along with the 2002.0 *XMM-Newton* OM *U*-band image and the 1996.6 *HST* WFPC1 red (F675W), Hα (F658N), *B*-band (F439W), and *U*-band (F336W) images. The MDM *R*-band image shows a bright source at the position of SN 1979C with a strength that suggests little change in *R*-band luminosity from that seen in the 1996.6 *HST* F675W images. Although the WFPC2 F675W and Harris *R* bandpasses are different in wavelength coverage (F675W bandpass: 6000–7500 Å; Harris *R* bandpass: 5600–8200 Å), they are both about equally sensitive to the strong and broad emission lines of [O I] $\lambda\lambda$6300, 6364, Hα, and [O II] $\lambda\lambda$7319, 7330, which dominate the late-time spectrum of SN 1979C (Fesen et al. 1999). This permits one to roughly equate these two filter images for the purposes of comparing total emission line levels in SN 1979C.

Relative flux measurements on the WFPC2-PC1 F675W and MDM *R*-band images of the SN 1979C source and several surrounding point sources, including the bright source 2.″0 nearly due east, were taken and indicate that SN 1979C's 2005.0 6000–7500 Å flux has remained constant to ± 0.25 mag from its 1996.6 level. Concerning the current level of Hα flux, the poor image quality of the MDM Hα image, differences in filter passbands between the WFPC2/F658N ($\lambda_0 = 6591$ Å; FWHM = 29 Å) and the MDM 8K/Hα filter ($\lambda_0 = 6565$ Å; FWHM = 80 Å), plus uncertainty as to the association of a strong, narrow Hα at the rest-frame velocity of M100 ($v = 1570$ km s^{-1}) with SN/CSM interaction make a definitive statement difficult. Nonetheless, the ground-based image data do suggest that considerable Hα emission currently exists at the SN 1979C site at a level consistent with that seen in the 1996.0 WFPC2-PC1 image (see Fig. 7, *right panel*).

4. DISCUSSION

4.1. *X-Ray Data*

SN 1979C is detected at a high flux level 23 yr after its outburst, with no indication of a decline over the last 6 years. This is in stark contrast to most other X-ray SNe, which typically show X-ray and radio rates of decline of $L_X \propto t^n$ with index n in the range 0.3–1.4 (see Immler & Lewin [2003] and Sramek & Weiler [2003] for review articles of the X-ray and radio rates of decline). The only SN that shows a similar persistent X-ray light curve is SN 1978K (Schlegel et al. 1999, 2004). Clearly, the high inferred flux is indicative of large amounts of shocked CSM and a high mass-loss rate in the scenario of the CSM being deposited by the progenitor.

Furthermore, our analysis may indicate a possible increase of the mass-loss rate for larger stellar wind ages if we assume a constant velocity forward shock. In order to check whether incorrect assumptions in the spectral properties of SN 1979C might mimic such an increase of the mass-loss rate, we investigated the effect of the assumed spectral parameters used for the conversion of source counts into fluxes. However, given our observed MOS count rates, we cannot find spectral templates with realistic plasma temperatures that could account for the apparent increase in the mass-loss rate. In fact, if we adopt a spectral template that only includes a hard thermal component with 10 keV for the forward shock emission for the earlier data for which no spectral information is available, the inferred flux would be 37% *lower* when compared to our two-temperature thermal emission model, which takes the emergence of the (softer) reverse shock into account. We therefore cannot reproduce a flat mass-loss rate history by changing the plasma temperatures of the shocked CSM alone.

Instead, we find that the mass-loss rate history is best represented by a constant stellar wind velocity and constant mass-loss rate by assuming that the shock front experienced a strong deceleration. Adopting deceleration parameters derived from VLBI imaging (with 9200 km s^{-1} for $t_w < 6$ yr, 6200 km s^{-1} for 6 yr $< t_w <$ 14 yr, and 5400 km s^{-1} for $t_w > 20$ yr; Marcaide et al. 2002) gives a flat (slope = 0) mass-loss rate history (see Fig. 5). This indicates that the assumed deceleration parameters are indeed plausible and contradicts claims of a free expansion based on the same VLBI data (Bartel & Bietenholz 2003).

The early upper limit from the merged *Einstein* data 0.66 yr after the outburst, however, is in conflict with a constant stellar wind velocity and constant mass-loss rate model (see Fig. 5). Similarly to SN 1979C, an early *ROSAT* upper limit to the X-ray flux of the SN Ic 1994I on day 52 has been reported to be in conflict with the X-ray evolution in terms of a simple power law and with a constant mass-loss rate and wind velocity (Immler et al. 2002). This suggests that a simple power-law model for the X-ray rate of decline might be incomplete for describing the early epoch in the CSM interaction. Assuming an initial exponential rise of the X-ray luminosity after the outburst (at time t_0) and a subsequent power-law decline with index s, we can parameterize the X-ray evolution as $f_X \propto (t - t_0)^{-s} e^{-\tau}$ with $\tau \propto (t - t_0)^{-\beta}$. This model has been successfully used to describe the time dependence of the radio emission of SNe (Weiler et al. 1986) and the X-ray emission of SN 1994I (Immler et al. 2002). In this representation, the external absorption of the emission is represented by the $e^{-\tau}$ term ("optical depth"), and the time dependence of the optical depth is parameterized by the exponent β. The rise of the X-ray flux could be due to a decreasing absorption by intervening material along the line of sight to the X-ray–emitting hot gas, or it could simply indicate a nonproduction of soft X-rays at early times. Unfortunately, the lack of high-quality data for SN 1979C at early times precludes a more detailed investigation. The low inferred mass-loss rate around 0.66 yr after the outburst of SN 1979C, however, could be due to such an exponential increase in the X-ray emission.

The data can therefore be reconciled with a constant mass-loss rate history if we assume an initial rise of the emission, which is observationally not further constrained.

Long-term X-ray light curves and high-quality spectra are also available for SNe 1993J (Immler et al. 2001; Zimmermann & Aschenbach 2003) and 1978K (Schlegel et al. 2004). While the overall X-ray light curve of SN 1993J is best described by a $t^{-0.3}$ rate of decline, significant "bumps" around day $\approx$1000 are observed, which might be due to a change in the slope of the CSM density profile (Zimmermann & Aschenbach 2003). VLBI imaging revealed that the expanding shock region has a circular morphology, which is indicative of a smooth CSM. Based on the X-ray and radio data, a significant change in the mass-loss rate of the SN 1993J progenitor was discovered, with a continuous decrease from $\dot{M} = 4\times10^{-4}$ to 4×10^{-5} $M_\odot$ yr^{-1} during the late stages of the evolution (Immler et al. 2001; van Dyk et al. 1994). This evolution has been interpreted as a transition in the progenitor's evolution from the red to the blue supergiant phase during the last $\approx$10,000 yr of the evolution (Immler et al. 2001). While a deceleration of the shock could not account for the change in the mass-loss rate history for SN 1993J, correction for a strongly decelerated shock produces a flat mass-loss rate history for SN 1979C with $\dot{M} \approx 1.5\times10^{-4}$ $M_\odot$ yr^{-1} (v_w/10 km s^{-1}). The bumpy CSM structure inferred for SN 1979C based on our analysis might be largely explained by systematic and statistical uncertainties in the X-ray flux, especially when the cross-calibration uncertainties between *Einstein*, *ROSAT*, *Chandra*, and *XMM-Newton* are taken into account (which would add an additional $\lesssim$10% to the errors quoted in this paper; see Snowden [2002] and the EPIC Calibration Documentation).[13] We therefore conclude that SN 1979C does not show any evidence for a change in the stellar wind parameters.

The X-ray spectrum of SN 1979C is best described by a two-temperature thermal plasma emission model with $kT_{\rm low} = 0.79^{+0.24}_{-0.17}$ and $kT_{\rm high} = 4.1^{+76}_{-2.4}$ keV, accounting for 64% and 36% of the total (0.3–2 keV) flux, respectively, and no intrinsic absorption. The hard and soft spectral components are likely due to emission from the forward (hard component) and reverse shock (soft component).

Similarly to SN 1979C, a best-fit two-temperature thermal plasma model with $kT_{\rm low} = 0.34 \pm 0.04$ and $kT_{\rm high} = 6.54 \pm 4$ keV was observed for SN 1993J based on high-quality *XMM-Newton* spectroscopy 8 yr after its outburst (Zimmermann & Aschenbach 2003). While these temperatures differ from the plasma temperatures found for SN 1979C, the overall temperature evolution for SN 1993J with a softening over time is consistent with the spectrum of SN 1979C at this late stage. Since no time-resolved spectroscopy is available for SN 1979C, we used the best-fit spectral template of the *XMM-Newton* MOS data to convert count rates into fluxes, luminosities, and compute mass-loss rates and CSM densities. Changes in the spectral properties, however, do not have a significant impact on the main results from this analysis (see § 2.1).

Chandra data of SN 1998S, which was observed to have a similarly high mass-loss rate (2×10^{-4} $M_\odot$ yr^{-1}), also showed a softening of its spectrum from 10.4 keV at day 678 after its outburst to 8.0 keV on day 1048 for a thermal plasma fit with Galactic absorption only (Pooley et al. 2002). A more recent *XMM-Newton* observation revealed the emergence of a soft ($\sim$0.8 keV) component, probably from the reverse shock, in addition to the harder component observed with *Chandra* (Immler & Lewin 2003).

[13] See http://xmm.vilspa.esa.es/external/xmm_sw_cal/calib/index.shtml.

In terms of spectral properties, SN 1979C shows a striking resemblance to SN 1978K. At an age of 24.2 yr, the X-ray spectrum of SN 1978K, as observed with *XMM-Newton*, was best-fitted with a two-temperature thermal plasma spectrum ($kT_{\rm low} = 0.61^{+0.04}_{-0.05}$ and $kT_{\rm high} = 3.16^{+0.44}_{-0.40}$ keV; Schlegel et al. 2004). Similarly to SN 1979C, SN 1978K shows no decline over the observed period and has been detected at a persistently high X-ray luminosity ($L_{0.5-2} = 1.5\times10^{39}$ ergs s^{-1}), which places both SNe into the category of strongly interacting with dense ambient CSM.

While minor contamination of the spectrum with unresolved XRBs within the disk of M100 cannot be conclusively excluded, spectral analysis of various point-source–free regions within the D_{25} ellipse of M100 give plasma temperatures significantly different from the spectral components above ($kT = 0.13 \pm 0.08$ keV) and likely originate in hot plasma within or above the disk of M100. Only high-resolution *Chandra* imaging spectroscopy with subarcsecond resolution could give a more definitive answers if the hard spectral component of the two-temperature fit is caused by XRBs within the *XMM-Newton* source extraction aperture or by thermal emission from shock-heated CSM by the forward shock of the SN. We also fitted single-component spectral models to the data, which give statistically acceptable fits and a similar temperature for the X-ray–emitting regions ($kT = 0.60^{+0.12}_{-0.19}$ keV for a thermal plasma fit; $kT = 0.53^{+1.40}_{-0.33}$ keV for a thermal bremsstrahlung fit). The absence of the hard spectral component could be interpreted as a lack of emission from the forward shock at late epochs in the CSM interaction.

Assuming a 0.6 keV thermal plasma spectrum (with absorbing column density fixed to the Galactic foreground column) gives a 23% lower flux compared to the two-temperature thermal plasma fit [$f_{0.5-2} = (1.8 \pm 0.2)\times10^{-14}$ ergs cm^{-2} s^{-1}]. The inferred lower mass-loss rate of $\dot{M} = (1.6 \pm 0.2)\times10^{-4}$ $M_\odot$ yr^{-1} is still consistent with the mass-loss rates at previous epochs and gives no evidence for an evolution of the progenitor in terms of stellar wind strength.

In order to compare the CSM properties in the vicinity of recent SNe for which sufficient data are available, we computed the CSM densities as a function of shell expansion radii for SN 1994I (Immler et al. 2002), SN 1993J (Immler et al. 2001), and SN 1978K (Schlegel et al. 2004) in an identical manner. While the CSM density profiles of SNe 1994I, 1993J, and 1978K can be fitted with a power law of the form $\rho_{\rm CSM} = \rho_0(r/r_0)^{-s}$ with $s = 1.9$ (SN 1994I), $s = 1.6$ (SN 1993J), and $s = 1.0$ (SN 1978K), we do not find a statistically acceptable fit for the CSM density profile using all the X-ray data of SN 1979C (see Table 3 and Fig. 6). If we only include the *ROSAT* HRI and *XMM-Newton* MOS detection (which have the highest signal-to-noise ratio), we obtain a best-fit CSM density profile of $\rho_{\rm CSM} = \rho_0(r/r_0)^{-s}$ with $s = 1.6 \pm 1.2$. Inclusion of the early *Einstein* upper limit gives a profile flatter than $s \lesssim 1.7$, consistent with the profile inferred from the *ROSAT* HRI and *XMM-Newton* MOS data. It should be noted, however, that cross-calibration uncertainties of $\lesssim$10% between the *XMM-Newton*, *ROSAT*, and *Einstein* fluxes have not been taken into account, which would increase the error to the CSM profile accordingly (see § 3.1).

While the CSM density profile is flat compared to SNe 1994I and 1993J, it is statistically consistent with a constant mass-loss rate and constant wind velocity profile. Within the errors, the two data points for the *ROSAT* PSPC and *Chandra* measurements are consistent with the CSM number density inferred from the *ROSAT* HRI and *XMM-Newton* MOS data, and close to the extrapolated CSM density profile of SN 1978K at these

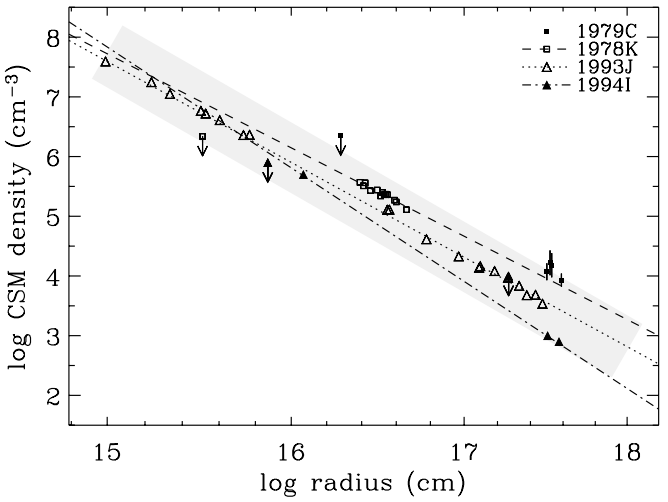

FIG. 6.—Circumstellar matter density profiles as a function of SN shell expansion radii for SNe 1994I (*filled triangles*; Immler et al. 2002), 1993J (*open triangles*; Immler et al. 2001), 1978K (*open squares*; this work), and 1979C (*filled squares*; this work). Error bars for SN 1979C are $\pm 1\ \sigma$. Best-fit CSM density profiles of $\rho_{\rm CSM} \propto r^{-s}$ with indices $s = -1.9$ (SN 1994I), $s = -1.6$ (SN 1993J), and $s = -1.0$ (SN 1978K) are drawn as lines.

large radii from the site of the explosion ($\log r[\rm cm] = 17.50$ and 17.59; see Fig. 6). A higher assumed wind velocity would further decrease the CSM number densities and give an even closer match to the extrapolated SN 1978K profile. Even though clumps in the CSM leading to an increase in the CSM density cannot be conclusively excluded, the seeming "jump" in the CSM density between $\log r(\rm cm) = 17.67$ (*ROSAT* PSPC) and 17.82 (*Chandra* ACIS data) is likely caused by the large errors associated with the low photon statistics of these observations and cross-calibration uncertainties between the different instruments.

Spatially resolved VLBI radio imaging of SN 1979C at an age of $t = 22$ yr have, in fact, shown a uniform shell-like structure with no evidence for a clumpy CSM or a geometry different from spherically symmetric (Bartel & Bietenholz 2003). Radio monitoring of SN 1979C over the past few decades has shown significant quasi-periodic or sinusoidal modulations in the radio flux (see Fig. 2 in Montes et al. 2000). These modulations in the radio light curve have been discussed in the context of a modulation of the stellar wind by a binary companion in a highly eccentric orbit (Weiler et al. 1992; Montes et al. 2000). The lack of a change in the radio spectral index over the monitored period, however, indicates an unchanged emission mechanism with constant efficiency (Montes et al. 2000). Our X-ray data do not support a substantial change in the CSM density profile, but they confirm a scenario in which the shock interacts with a dense CSM ($\gtrsim 10^4$ cm^{-3}).

4.2. *Optical/UV Data*

Late-time optical and UV photometry and spectroscopy can yield interesting insights into the CSM properties, such as electron densities, shock velocities, and ionization states of the shocked CSM. From these, conclusions can be drawn about the nature and mass of the progenitor, as well as on its evolution. Of particular interest are the late-time optical and UV emission as a result of radiative cooling of the SN shock, ionized by incident X-rays from the CSM shock interaction and by the SN event itself (Chevalier & Fransson 1994).

Multiband *HST* imaging of the environment of SN 1979C was successfully used to recover optical emission from SN 1979C at $t \approx 20$ yr after its outburst (van Dyk et al. 1999). The *HST* data showed SN 1979C to be a bright source within a small ($\lesssim 1''$) stellar cluster of red supergiants and young blue stars. While SN 1979C had magnitudes of $m_U = 23.2$, $m_B = 23.3$, $m_V = 22.1$, and $m_I = 21.0$ mag, the next brightest optical/UV sources in the immediate environment had $m_V \gtrsim 24$ and $m_I \gtrsim 23$ mag. The *HST* images further suggest the presence of 5–7 additional, although faint, UV-emitting stars at the site. Three more UV sources were imaged with the *HST* further to the east ($\approx 2''$), which are located within the OM counts extraction aperture ($2''.9$ radius). It is therefore possible that these sources contribute a significant fraction to the observed optical/UV flux within the extracted aperture.

The new ground-based *R*-band and Hα images taken in 2004 December, some 25.6 yr after the outburst, continue to indicate a strong CSM interaction, 3 yr after the *XMM-Newton* observations. This suggests that both Hα and the broad [O I] and [O II] line emissions seen in the 1993 spectra are still of comparable strength to levels more than a decade earlier.

Little is known to date about the late-time spectra of SNe shortward of 5000 Å. UV emission is detected from the position of SN 1979C with a UVW1-band luminosity of $L_{\rm UVW1} = 9 \times 10^{36}$ ergs s^{-1}. Comparison of the Hα and UV luminosities of SN 1979C show an interesting similarity ($L_{\rm H\alpha} = 1.6 \times 10^{37}$ ergs s^{-1}; van Dyk et al. 1999). The Hα light curve of SN 1979C shows no decline between 1987 and 1991 (Fesen et al. 1999), while a slight increase in the 1993 data is observed, which coincides with the observed flattening of the radio light curve. A similar Hα luminosity was observed for the Type II-L SN 1980K (2.5×10^{37} ergs s^{-1}; Fesen et al. 1999) at an age of 14–15 yr after its explosion. These high late-time Hα luminosities are largely the result of high electron densities ($n_e \gtrsim 10^4 - 10^5$ cm^{-3}), which are supported by the high inferred CSM densities in this paper ($\gtrsim 10^4$ cm^{-3}).

The OM *U*-band data show a bright source at the position of SN 1979C ($L_U = 5 \times 10^{36}$ ergs s^{-1}), while the *HST* data from 1996 show very weak emission from SN 1979C in the *U* band. This difference can be attributed to the cutoff of the *HST U*-band filter redward to 3800 Å, while the *U*-band filter of the OM cuts off at 3950 Å, which then includes the broad [Ne III] emission lines at $\lambda\lambda$3868, 3869. The detection of [Ne III] emission lines from SN 1979C (Fesen et al. 1999) may explain why the SN is brighter in the *XMM-Newton* OM *U*-band images than in the *HST U*-band (F336W filter) images.

The peak surface brightness of the OM *U*-band emission coincides with the peak in the *R* band (see Fig. 7), which includes broad Hα, [O II] $\lambda\lambda$7319, 7330, and [O I] $\lambda\lambda$6300, 6364 line emission from the SN ejecta and narrow Hα, presumably associated with the strong CSM interaction. While the source at the position of SN 1979C is classified as pointlike in all OM bands by the source detection routines, slightly more extended emission is visible in the OM *B*- and UVW1-band images compared to the *U* band. This is consistent with at least a substantial fraction of the *B*-band, *U*-band ($\lesssim 30\%$) and UVW1-band ($\gtrsim 50\%$) fluxes being to the SN itself. For the UVW1 band, most of the flux likely arises from Mg II 2800 Å where the peak in the UVW1-band effective area is located. A substantial fraction of the *B*-band flux might also be due to SN 1979C (20%–30% contribution to the total light in this OB/SN spatial region) and is due to [O III] 4363 Å line emission. The contribution from the OB stars to the east may be significantly reduced, relative to that from the SN, to the total flux within the *U*-band passband for both the *HST* and OM filters, due to the Balmer jump at 3600 Å in the stellar spectra of these stars.

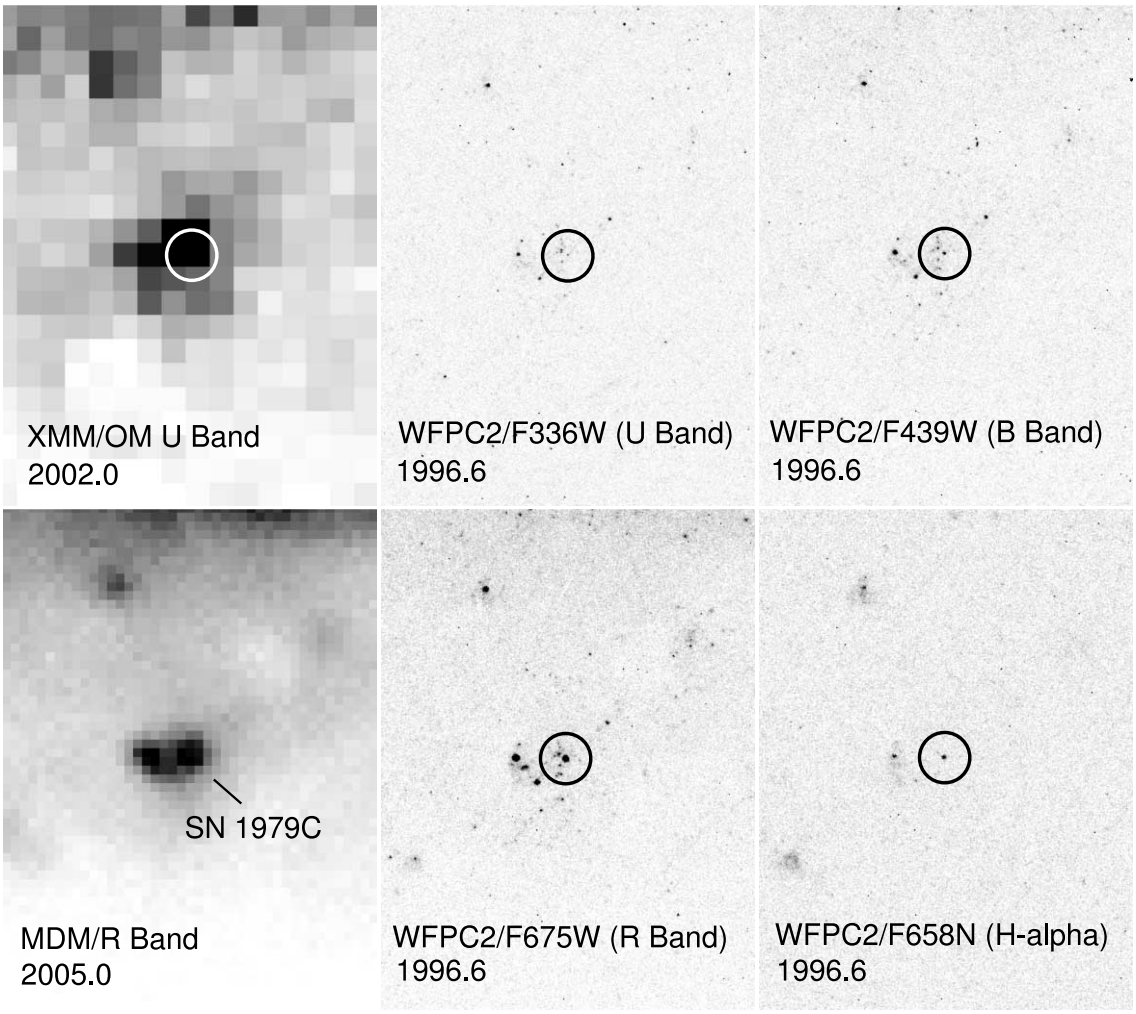

FIG. 7.—*XMM-Newton* OM *U*-band image (from 2001 December 28; *top left panel*), MDM *R*-band image (from 2004 December 19 and 20; *bottom left panel*), and *HST* WFPC2-PC1 U, B, R-band and Hα images (from 1996 July 29; *middle and right panels*) of the SN 1979C region. The circles (radius 1″) are at the *HST R*-band centroid position of SN 1979C.

Because of the strong appearance of SN 1979C in the OM *U*-band image, the [Ne III] emission may have substantially increased in strength since the *HST* spectra obtained in 1996 (Fesen et al. 1999). It should be kept in mind, however, that the *HST* data were acquired before the increase of SN 1979C at radio wavelengths. This increase could be caused by either a higher ionization of the CSM interaction and/or a lowering of the local reddening/extinction due to dust evaporation via shocks (i.e., dust in the CSM) or less ejecta formed dust via dilution from expansion.

In summary, the high inferred optical/UV flux for SN 1979C, especially in the *U* band, further suggests continued strong CSM interaction even at this late stage in the evolution and large radii from the site of the explosion, which is also supported by our recent MDM *R*-band data, and confirms our results, which are independently inferred from the X-ray data.

5. SUMMARY

In this paper we present a comprehensive study of the Type II-L SN 1979C in X-rays and in the optical/UV based on *XMM-Newton* data, all archival X-ray data available to date, as well as archival optical data from the *HST* and a recent MDM observation. Key findings are as follows.

1. SN 1979C is observed at a high X-ray luminosity 23 yr after its outburst ($L_{0.3-2} = 8\times10^{38}$ ergs s^{-1}) and shows no evidence for a decline over the observed period of 16–23 yr after its outburst.

2. The X-ray spectrum, measured for the first time, gives a best-fit two-temperature thermal plasma model with $kT_{\rm low} = 0.79^{+0.24}_{-0.17}$ keV, $kT_{\rm high} = 4.1^{+76}_{-2.4}$ keV, and Galactic absorption only, characteristic for emission from both the forward (hard component) and reverse shock (soft component). The spectral properties are similar to that of other core-collapse SNe, such as SNe 1978K and 1993J.

3. After correction for a decelerating shock front, we find no evidence for a change in the progenitor's mass-loss rate ($\dot{M} \approx 1.5\times10^{-4}\ M_\odot$ yr^{-1}) over a period of $\gtrsim$16,000 yr in the stellar evolution of the progenitor.

4. High CSM number densities ($\gtrsim10^4$ cm^{-3}) are inferred for SN 1979C even at large radii (out to $\approx4\times10^{17}$ cm) from the site of the explosion, similar to SN 1978K. The CSM density profile can be fitted with a power law of the form $\rho_{\rm CSM} = \rho_0(r/r_0)^{-s}$ with index $s \lesssim 1.7$ comparable to other SNe (e.g., SNe 1994I and 1993J) and support a constant mass-loss rate and a constant stellar wind velocity.

5. A pointlike optical/UV source is detected at the position of SN 1979C with the Optical Monitor on board *XMM-Newton*, with *U*-, *B*-, and UVW1-band luminosities of $L_U = 5\times10^{36}$, $L_B = 7\times10^{36}$, and $L_{\rm UVW1} = 9\times10^{36}$ ergs s^{-1}, similar to its Hα and *R*-band luminosity. The high luminosities, especially in the *U* band arising from Mg II 2800 Å and in the UVW1 band from [Ne III]

$\lambda\lambda$3868, 3869 emission lines, indicate substantial CSM interaction in the late-time evolution of SN 1979C and independently support the strong observed CSM interaction as observed in X-rays.

This paper is based on observations obtained with *XMM-Newton*, an ESA science mission with instruments and contributions directly funded by ESA Member States and NASA. The research has made use of data obtained through the High Energy Astrophysics Science Archive Research Center Online Service, provided by the NASA/Goddard Space Flight Center. K. W. W. wishes to thank the Office of Naval Research (ONR) for the 6.1 funding supporting his research.

REFERENCES

Bartel, N., & Bietenholz, M. F. 2003, ApJ, 591, 301
Chevalier, R. A., & Fransson, C. 1994, ApJ, 420, 268
Crotts, A. P. S. 2001, BAAS, 33, 792
Dickey, J. M., & Lockman, F. J. 1990, ARA&A, 28, 215
Fesen, R. A., & Matonick, D. M. 1993, ApJ, 407, 110
Fesen, R. A., et al. 1999, AJ, 117, 725
Fransson, C., Lundqvist, P., & Chevalier, R. A. 1996, ApJ, 461, 993
Freedman, W. L., et al. 1994, Nature, 371, 757
Immler, S., Aschenbach, B., & Wang, Q. D. 2001, ApJ, 561, L107
Immler, S., & Lewin, W. H. G. 2003, in Supernovae and Gamma-Ray Bursters, ed K. Weiler (Berlin: Springer), 91
Immler, S., Pietsch, W., & Aschenbach, B. 1998, A&A, 331, 601
Immler, S., Wilson, A. S., & Terashima, Y. 2002, ApJ, 573, L27
Kaaret, P. 2001, ApJ, 560, 715
Marcaide, J. M., et al. 2002, A&A, 384, 408
Mattei, J., Johnson, G. E., Rosino, L., Rafanelli, P., & Kirschner, R. 1979, IAU Circ., 3348, 1
Montes, M. J., Weiler, K. W., Van Dyk, S. D., Panagia, N., Lacey, Ch. K., Sramek, R. A., & Park, R. 2000, ApJ, 532, 1124
Pooley, D., et al. 2002, ApJ, 572, 932
Ray, A., Petre, R., & Schlegel, E. M. 2001, AJ, 122, 966
Schlegel, E. M., Kong, A., Kaaret, P., DiStefano, R., & Murray, S. 2004, ApJ, 603, 644
Schlegel, E. M., Ryder, S., Staveley-Smith, L., Petre, R., Colbert, E., Dopita, M., & Campbell-Wilson, D. 1999, AJ, 118, 2689
Snowden, S. L. 2002, in Proc. ESTEC Symp., New Visions of the X-Ray Universe in the *XMM-Newton* and *Chandra* Era (ESA SP-488; Noordwijk: ESA), in press (astro-ph/0203311)
Sramek, R. A., & Weiler, K. W. 2003, in Supernovae and Gamma-Ray Bursters, ed K. Weiler (Berlin: Springer), 145
van Dyk, S. D., Weiler, K. W., Sramek, R. A., Rupen, M. P., & Panagia, N. 1994, ApJ, 432, L115
van Dyk, S. D., et al. 1999, PASP, 111, 313
Weiler, K. W., Panagia, N., Sramek, R. A., van Dyk, S. D., Montes, M. J., & Lacey, Ch. K. 2001, in Supernovae and Gamma-Ray Bursts, ed. M. Livio, N. Panagia, & K. Sahu (Cambridge: Cambridge Univ. Press), 198
Weiler, K. W., Sramek, R. A., Panagia, N., van der Hulst, J. M., & Salvati, M. 1986, ApJ, 301, 790
Weiler, K. W., van Dyk, S. D., Discenna, J. L., Panagia, N., & Sramek, R. A. 1991, ApJ, 380, 161
Weiler, K. W., van Dyk, S. D., Pringle, J. E., & Panagia, N. 1992, ApJ, 399, 672
Zimmermann, H.-U., & Aschenbach, B. 2003, A&A, 406, 969